Research Paper
J. Astron. Space Sci. 32(4), 289-295 (2015)
http://dx.doi.org/10.5140/JASS.2015.32.4.289

JASS Journal of Astronomy and Space Sciences

Localization of Ultra-Low Frequency Waves in Multi-Ion Plasmas of the Planetary Magnetosphere

Eun-Hwa Kim[1†], Jay R. Johnson[1], Dong-Hun Lee[2]

[1]Princeton Center for Heliophysics and Princeton Plasma Physics Laboratory, Princeton University, Princeton, NJ 08543-0451, USA

[2]School of Space Research, Kyung Hee University, Yongin 17104, Korea

By adopting a 2D time-dependent wave code, we investigate how mode-converted waves at the Ion-Ion Hybrid (IIH) resonance and compressional waves propagate in 2D density structures with a wide range of field-aligned wavenumbers to background magnetic fields. The simulation results show that the mode-converted waves have continuous bands across the field line consistent with previous numerical studies. These waves also have harmonic structures in frequency domain and are localized in the field-aligned heavy ion density well. Our results thus emphasize the importance of a field-aligned heavy ion density structure for ultra-low frequency wave propagation, and suggest that IIH waves can be localized in different locations along the field line.

Keywords: ultra-low frequency waves, electromagnetic ion cyclotron waves, ion-ion hybrid resonance, mode conversion, wave-wave interaction

1. INTRODUCTION

Plasmas support a wide variety of plasma waves that carry information to remote observers (Lee et al. 2014; Hwang 2015). Ultra-Low Frequency (ULF) waves in the ion cyclotron range of frequency, which can interact with electrons and ions (Rauch & Roux 1982; Horne & Thorne 1997; Song et al. 1999), are often observed in planetary magnetospheres (Russell et al. 2008; Boardsen et al. 2012) as well as in Earth's magnetosphere and ionosphere (Kim et al. 2010, 2011b).

In the ion cyclotron frequency range, the wave dispersion relations can be simplified to

$$n_{\perp}^2 \cong \frac{(\varepsilon_R - n_{\parallel}^2)(\varepsilon_L - n_{\parallel}^2)}{(\varepsilon_S - n_{\parallel}^2)} \tag{1}$$

where n is the wave refractive index (kc/ω), and subscripts $\perp$ and $\parallel$ represent the perpendicular and parallel directions to the ambient magnetic field (B_0), respectively. $\varepsilon_{R,L,S}$ are the tensor elements for multiple ions,

$$\varepsilon_R(\varepsilon_L) \cong \frac{1}{\omega}\frac{\omega_{pe}^2}{\Omega_e}\left[\pm 1 - \sum_{ion}\frac{\eta_j \Omega_j}{\omega \pm \Omega_j}\right] \tag{2}$$

and

$$\varepsilon_S \cong \frac{\omega_{pe}^2}{\Omega_e}\sum_{ion}\frac{\eta_j \Omega_j}{\Omega_j^2 - \omega^2} \tag{3}$$

where $\omega = 2\pi f$ is the angular frequency, $\omega_{pj(e)}$ and $\Omega_{j(e)}$ are the plasma and cyclotron frequencies of jth ion (electron), respectively, and $\eta_{ion} = N_{ion}/N_e$ is the ratio of the ion density (N_{ion}) to electron density (N_e).

For perpendicular propagation ($n_{\parallel} \to 0$), the dispersion relation in Eq. (1) exhibits a resonance ($n_{\perp} \to \infty$) where $e_S(\omega_{bb}) = 0$,

$$\omega_{bb}^2 = \Omega_1 \Omega_2 \frac{\eta_1 \Omega_2 + \eta_2 \Omega_1}{\eta_1 \Omega_1 + \eta_2 \Omega_2} \tag{4}$$

which is the Buchsbaum frequency (bi-ion frequency)

Received Nov 19, 2015 **Revised** Dec 3, 2015 **Accepted** Dec 4, 2015

†**Corresponding Author**
E-mail: ehkim@pppl.gov, ORCID: 0000-0001-6179-4666
Tel: +1-609-243-3147, Fax: +1-609-243-2662

(Buchsbaum 1960). For oblique propagation ($n_{\|} \neq 0$), the perpendicular resonance ($n_{\perp} \rightarrow \infty$) occurs at the location ($\omega_{ii}(x) = \omega$) where

$$n_{\|}^2(\omega = \omega_{ii}) = \varepsilon_S(\omega = \omega_{ii}) \quad (5)$$

Between each pair of gyrofrequencies, there is a mode conversion location that is referred to as the Ion-Ion Hybrid (IIH) resonance, with a corresponding frequency (ω_{ii}) called the IIH frequency (Lee et al. 2008). When Fast compressional Waves (FWs), propagating across magnetic flux surfaces and satisfying the IIH resonance condition, encounter inhomogeneity for the heavy ion concentration and/or magnetic field strength, it may be possible for the wave to satisfy the resonance condition (5), where energy from incoming FWs concentrates at the IIH resonance location and the mode converts to field-aligned propagating IIH waves that satisfy the dispersion relation of $n_{\|}^2 \sim \varepsilon_S$.

The IIH resonance can exhibit significant differences because of the different conditions in planetary magnetospheres. For Mercury, where the magnetic field is relatively weak, the wavelength of field-aligned modes can be comparable to the size of the magnetosphere. Therefore, IIH waves oscillate globally along the magnetic field lines for Mercury, similar to the field line resonance on Earth (Othmer et al. 1999; Glassmeier et al. 2003, 2004; Klimushkin et al. 2006; Kim et al. 2008, 2011a, 2013, 2015a, b). On the other hand, on Earth, the magnetic field strength is larger and the wavelength is shorter, which typically localizes mode converted waves between the Buchsbaum cutoff locations, which occur at around 10 degrees latitude. The modes that result from mode conversion are typically linearly polarized ElectroMagnetic Ion Cyclotron (EMIC) waves, which can be generated via mode conversion near the IIH resonance location (Lee et al. 2008). These waves have a significantly different polarization from EMIC waves, which are excited by proton temperature anisotropy (Cornwall 1965; Kennel & Petschek 1966; Williams & Lyons 1974a, b; Taylor & Lyons 1976). Because the incoming FW absorption at the IIH resonance (the generation of linearly polarized EMIC waves) occurs at a limited wave frequency and heavy ion density ratio, linearly polarized waves can be used as a diagnostic tool to estimate the heavy ion density ratio (Kim et al. 2015c).

In planetary magnetospheres, as the mode-converted IIH waves near the magnetic equator propagate to higher magnetic latitudes, the waves reach cutoff ($n_{\|} = 0$ and $\varepsilon_S = 0$) at $\omega = \omega_{bb}$ and parallel resonance ($n_{\|} \rightarrow \infty$ and $\varepsilon_S \rightarrow \infty$) locations at $\omega = \Omega_{ion}$. Because the IIH waves are partially reflected at the Buchsbaum resonance location where $\omega = \omega_{bb}$, the waves are possibly localized near the magnetic equator between two Buchsbaum resonance locations (Klimushkin et al. 2010; Vincena et al. 2011). The localization of mode-converted IIH waves is referred to as IIH Alfven resonance, and is experimentally detected in laboratory plasmas (Vincena et al. 2011, 2013; Farmer & Morales 2014).

Recent 2D full wave simulations of Mercury's dipolar magnetosphere (Kim et al. 2015a), which assumed constant particle densities, clearly showed the reflection of the IIH resonant waves at the Buchsbaum resonance location and wave tunneling through the wave stopgap between cutoff and resonance. However, as shown in Eq. (4), the Buchsbaum frequency is a function of the heavy ion density concentration ratio as well as the ambient magnetic field strength. Therefore, it is useful to examine the solutions of IIH resonant waves in more detail to determine how the wave structure and absorption of energy depend on variations in the magnetic field strength and density.

In this paper, we use a multi-ion fluid wave code to demonstrate mode conversion that occurs at the IIH resonance when impulsive FWs enter the plasma with a 2D inhomogeneous density structure, which is assumed to result from the sputtering of material from the surface of Mercury. We find that mode converted IIH waves can be localized in the density well along the magnetic field line, and also exhibit harmonic frequency structure.

2. NUMERICAL RESULTS

We employ the fluid wave simulation model developed by Kim & Lee (2003). Similar to previous wave simulations (Kim et al. 2008, 2013), we adopt the plasma conditions present on Mercury, and thus the background magnetic field (B_0 = 86 nT) and the electron density (N_e = 3 cm^{-3}) are assumed to be constant. The ambient magnetic field lies in the Z direction and the inhomogeneity is introduced in the x-z plane. We limit ourselves in that all perturbations are proportional to $\exp(ik_y y)$, where k_y is the given wavenumber in the y direction and, for the sake of simplicity, is assumed to be 0. Because the magnetopause of Mercury is located near 1.4 R_M (Anderson et al. 2011), we assume a shorter radial distance of 1 R_M than the magnetopause location in the X direction, where R_M is the radius of Mercury. The length in the Z direction (L_z) is assumed to be 0.93 R_M, which is similar to field line length at L_M = 1.5 in dipole coordinates, where L_M is the magnetic L-shell number for Mercury. We adopt a grid with dimensions $N_x \times N_z$ = 300×100, and to save computing time, the ratio of proton mass (m_H) to electron mass (m_e) is assumed to be 100 (m_H/m_e = 100).

Because sodium is one of the major heavy ions on Mercury (Zurbuchen et al. 2011; Raines et al. 2014), we adopt an electron-proton-sodium plasma, similar to previous numerical studies (Kim et al. 2008, 2011a). We assume the sodium density (N_{Na}) has a minimum value (i.e., sodium density well) at the center of the simulation domain, as shown in Fig. 1. The electron density is assumed to be the sum of the ion densities. Thus, the ratio of the proton density to electron density is $\eta_H = N_H/N_e = 1 - \eta N_a$, where $\eta N_a = N_{Na}/N_e$, and η_H is maximum in the middle of the simulation domain.

The simulation is driven by imposing an impulse in E_y at $X = x/L_x = 1$ during the interval $0 \le \tau = t/t_{ci} \le 2.5$, where $t_{ci} = 2\pi/\Omega_H$, as shown in Fig. 2(a) and 2(b) shows the initial field-aligned wave structures along $Z = z/L_z$ at $X = 1$. Because the width of the source is closely related to the initial wavevector, a wide source corresponds to a more perpendicular propagation. The boundaries become perfect reflectors after the impulsive stimulus ends ($\tau = 2.5$), and thus the total energy in the box model will remain constant in time after this interval.

We stored the time history of the electromagnetic fields at each grid point (X, Z) during the simulation run time ($0 < \tau < 55$) and obtained the wave power spectra using a fast Fourier transform. To examine wave properties along and across the magnetic field line, we selected two points in X and Z, with $X_0 = 0.55$ and $Z_0 = 0.7$, as shown in Fig. 1. Under the given conditions, and because the density inhomogeneity lies in the X and Z directions, E_x represents the mixture of the IIH resonant wave and FW modes, while E_y shows the pure FW mode.

Figs. 3(a) and 3(b) show the time history of the transverse component of B_0 of the electric fields (E_x and E_y) along X at $Z = Z_0$. In this figure, the FWs launched at $X = 1$ propagate toward the Na^+ density well and reach the inner boundary at $X = 0$. The evidence of a wave stopgap and wave tunneling near $X \approx 0.5$ at $Z = 0.55$ are also found in E_y. On the other hand, as soon as the FW packet reaches the region $0.5 < X < 1$, the IIH resonant wave modes exhibit standing oscillations in Ex and the period of the oscillation decreases as X decreases (decreasing η_{Na} concentration). However, for $X < 0.5$, no oscillation of the mode-converted waves is found in E_x.

The wave time history along the Z direction at $X = X_0$ is plotted in Figs. 3(c) and 3(d). In this case, the FWs in the E_y component reach the boundaries in a short time and reflect. In this figure, it can be seen that E_y in each location along Z has a different period of wave oscillation. Near the boundaries, E_y exhibits a mixture of long and short period waves, while long period waves only appear near the center of the Z direction. On the other hand, waves with E_x polarization are localized to within the middle of Z. As shown in Figs. 3(a) and 3(b), the wave periods at $Z = 0.55$ are lower than at $Z = 0.7$.

Fig. 4 shows the wave spectra of E_x and E_y. E_x in Figs. 4(a) and 4(b) shows a strong continuous band at the IIH resonance wave in the X direction, which is consistent with previous numerical results. Because the field-aligned wavenumber is not fixed, several harmonics of the IIH waves can be seen. The wave power spectra along Z in Figs. 4(c) and 4(d) also clearly show that the mode-converted IIH waves have several eigenfrequencies and are localized

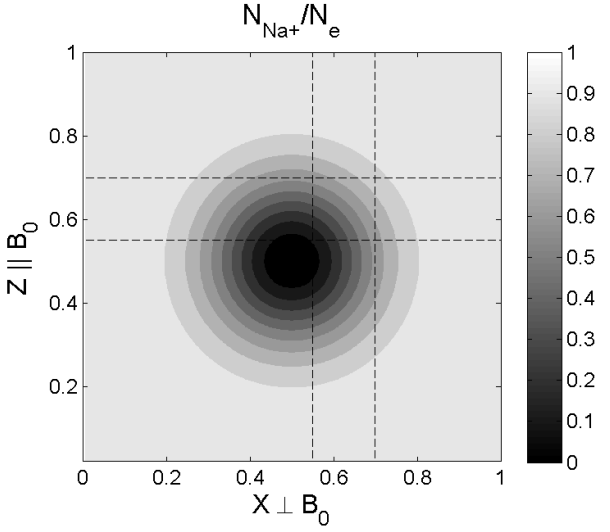

Fig. 1. Ratio of Na^+ density to the electron density in the *X-Z* plane. The sodium concentration has a minimum at the center of the simulation domain. The dashed lines show selected locations of X and *Z*; X_0 (Z_0) = 0.5 and 0.7 for Figs. 3 and 4.

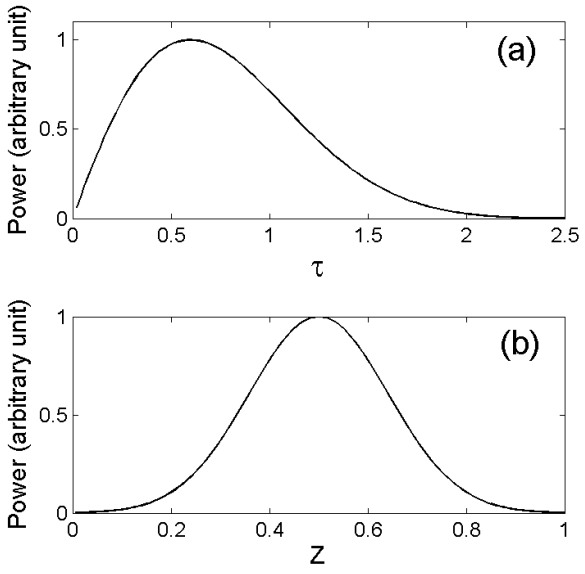

Fig. 2. Adopted impulsive input (a) in time and (b) in space.

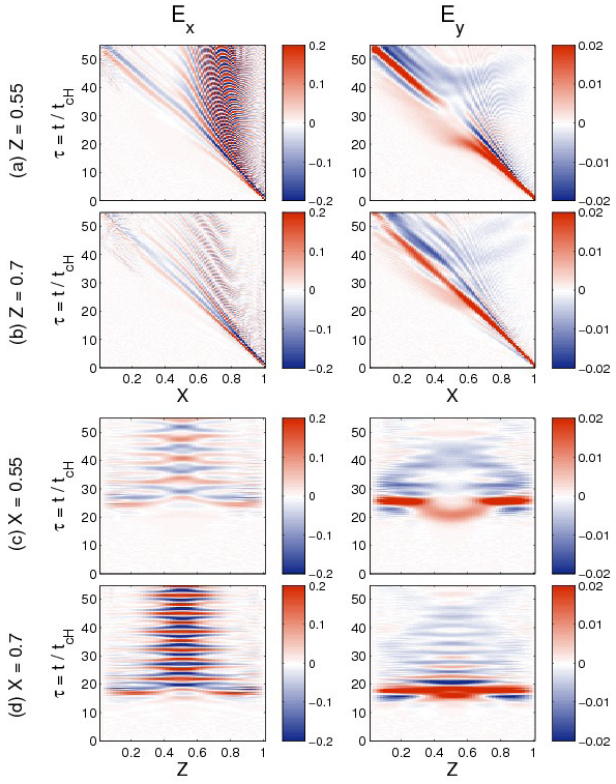

Fig. 3. Wave time histories of E_x and E_y along X for (a) $Z = 0.55$ and (b) $Z = 0.7$ and along Z for (c) $X = 0.55$ and (b) $X = 0.7$, respectively.

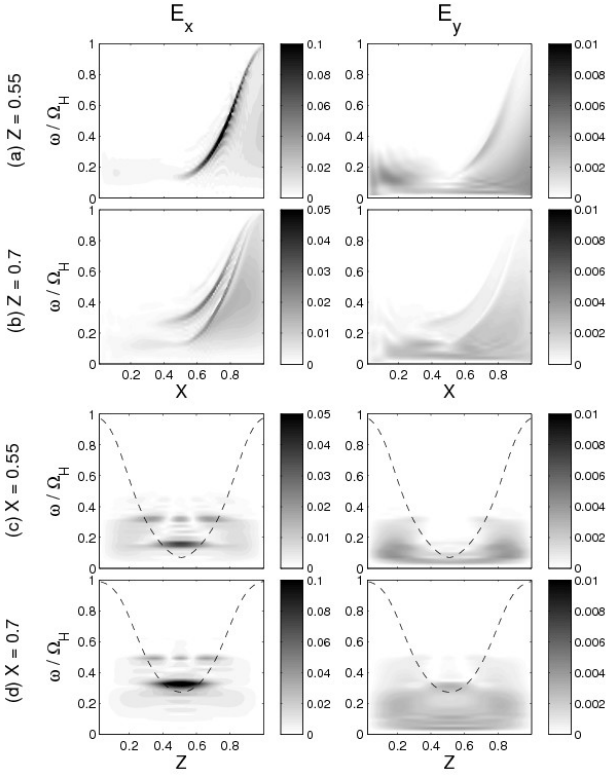

Fig. 4. Wave spectra of the E_x and E_y components along X for (a) $Z = 0.55$ and (b) $Z = 0.7$ and along Z for (c) $X = 0.55$ and (d) $X = 0.7$, respectively. Dashed lines represent the calculated Buchsbaum frequencies along Z.

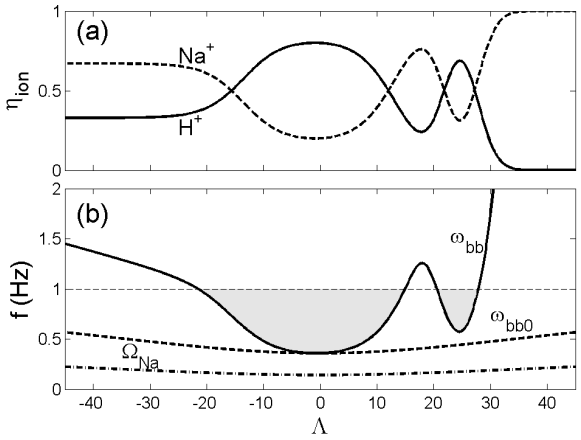

Fig. 5. (a) Arbitrary H^+ and Na^+ density ratios along the magnetic field line at $L_M = 2$; (b) the solid line is the calculated Buchsbaum frequency along the magnetic field line by adopting the heavy ion density ratio from (a), the dashed line is the Buchsbaum frequency for $\eta_{Na} = 20\%$, and the dashed-dotted line is the sodium gyrofrequency. Here, the gray-filled area is where an IIH wave with 1 Hz can propagate; thus, IIH waves generated near the magnetic equator can be localized between $-21.7 < \Lambda < 15$ and $20.5 < \Lambda < 27.9$.

between the two Buchsbaum resonance locations. The second harmonic of the IIH waves has a node near $Z = 0.55$ and an antinode near $Z = 0.7$; therefore, E_x only shows a strong fundamental band in Fig. 4(a) but strong fundamental and second harmonics in Fig. 4(b).

The FWs in the E_y component propagate to the middle of the simulation domain and energy in high frequencies, where the strong continuous band appears in E_x, cannot reach the inner boundary at $X = 0$. The inaccessibility occurs because FWs propagating from Na^+-rich to H^+-rich plasma directly encounter the IIH resonance location where strong energy absorption occurs (up to 100% as predicted by Lee et al. 2008). For waves with $\omega/\Omega_H < 0.3$, the FWs are partially absorbed at the IIH resonance location and the rest of the energy can reach the FW cutoff locations where $n_{\parallel}^2 = \varepsilon_L$, and then encounter another IIH resonance location at $X < 0.5$. However, when waves propagate from H^+-rich to Na^+-rich plasma, wave absorption only occurs in the limited frequencies and the absorption coefficient is much lower than that of the opposite case, with no continuous band at the IIH resonance appearing.

3. DISCUSSION

In this paper, we show how mode-converted IIH waves can be localized in a heavy ion density well in slab coordinates. Because the Buchsbaum frequency increases as the heavy ion density concentration ratio increases, an irregular ion density structure along the field line can lead to an asymmetric

structure of the Buchsbaum frequency. Our results, therefore, emphasize the importance of field-aligned heavy ion density structures for ULF wave propagation. It should be noted that equilibria in magnetospheres with rotational disks generally have density structures along the magnetic field lines due to centrifugal acceleration, which concentrates the heavy ions into the magnetodisk.

In Fig. 5, we demonstrate how asymmetry in the ion density ratio affects the field-aligned wave propagation. We assumed the field-aligned density structure of η_{Na} and η_{H} at Mercury, as shown in Fig. 5(a), and calculated the Buchsbaum frequency, as shown in Fig. 5(b). When plasma contains a constant sodium density of η_{Na} = 20% and the Buchsbaum frequency (ω_{bb0}), wave frequencies that are higher than the highest Buchsbaum frequency do not encounter the cutoff condition, and thus can globally oscillate in a manner similar to the field-line resonance on Earth (Lee & Lysak 1989). However, for an asymmetric structure of the ion density, waves generated near the magnetic equator with 1 Hz can be localized between -21.7 < Λ < 15. In addition, if the waves can tunnel through the small bump of the Buchsbaum frequency, the waves can reach the secondary density well and are possibly localized between 20.5 < Λ < 27.9.

Interestingly, the Buchsbaum resonance is also a cutoff condition of the Left-Hand Polarization (LHP) EMIC waves (Johnson et al. 1995). In Earth's magnetosphere, as these waves propagate along B_0, the wave normal angle increases and becomes nearly 90° when waves reach the Buchsbaum resonance. The waves then reflect toward a higher L-shell and lower magnetic latitude (Kim & Johnson 2015). Because both reflected IIH waves (Kim et al. 2015a) and LHP EMIC waves (Kim & Johnson 2015) at the Buchsbaum resonance propagate to the different L-shells in the dipole field configuration, how 2D/3D heavier ion density structures in the planetary magnetosphere relate to propagation characteristics of the IIH and LHP EMIC waves remains as future work.

In summary, we investigate how mode-conversion at the IIH resonance occurs when heavy ion density has transverse and longitudinal inhomogeneity in slab coordinates. The multi-ion simulation results show that the IIH waves have a continuous band across the field line, which is consistent with previous numerical studies. These waves also have harmonic structures in frequency domain and are also localized in the field-aligned heavy ion density well.

ACKNOWLEDGMENTS

The work at the Princeton University was supported by NASA grants (NNH09AM53I, NNH09AK63I, NNH11AR07I, NNX14AM27G, and NNH14AY20I), NSF grant ATM0902730, AGS-1203299, and DOE contract DE-AC02-09CH11466. This work was facilitated by the Max Planck/Princeton Center for Plasma Physics. The work at the Kyung Hee University was also supported by the BK21 Plus Program through the National Research Foundation of Korea, funded by the Ministry of Education, Science and Technology.

REFERENCES

Anderson BJ, Johnson CL, Korth H, Purucker ME, Winslow RM, et al., The Global Magnetic Field of Mercury from MESSENGER Orbital Observations, Science 333, 1859-1862 (2011). http://dx.doi.org/10.1126/science.1211001

Boardsen SA, Slavin JA, Anderson BJ, Korth H, Schriver D, et al., Survey of coherent ~1 Hz waves in Mercury's inner magnetosphere from MESSENGER observations, J. Geophys. Res. 117, A00M05 (2012). http://dx.doi.org/10.1029/2012JA017822

Buchsbaum SJ, Ion Resonance in a Multicomponent Plasma, Phys. Rev. Lett. 5, 495-497 (1960). http://dx.doi.org/10.1103/PhysRevLett.5.495

Cornwall JM, Cyclotron instabilities and electromagnetic emission in the ultra low frequency and very low frequency ranges, J. Geophys. Res. 70, 61-69 (1965). http://dx.doi.org/10.1029/JZ070i001p00061

Farmer WA, Morales GJ, The ion-ion hybrid Alfvén resonator in a fusion environment, Phys. Plasmas 21, 062507 (2014). http://dx.doi.org/10.1063/1.4882662

Glassmeier KH, Mager PN, Klimushkin DY, Concerning ULF pulsations in Mercury's magnetosphere, Geophys. Res. Lett. 30, 1928 (2003). http://dx.doi.org/10.1029/2003GL017175

Glassmeier KH, Klimushkin D, Othmer C, Mager P, ULF waves at Mercury: Earth, the giants, and their little brother compared, Adv. Space Res. 33, 1875-1883 (2004). http://dx.doi.org/10.1016/j.asr.2003.04.047

Horne RB, Thorne RM, Wave heating of He+ by electromagnetic ion cyclotron waves in the magnetosphere: Heating near the H+ - He+ bi-ion resonance frequency, J. Geophys. Res. 102, 11457-11471 (1997). http://dx.doi.org/10.1029/97JA00749

Hwang KJ, Magnetopause Waves Controlling the Dynamics of Earth's Magnetosphere, J. Astron. Space Sci. 32, 1-11 (2015). http://dx.doi.org/10.5140/JASS.2015.32.1.1

Johnson JR, Chang T, Crew GB, A study of mode conversion in an oxygen–hydrogen plasma, Phys. Plasmas 2, 1274-1284 (1995). http://dx.doi.org/10.1063/1.871339

Kennel CF, Petschek HE, Limit on stably trapped particle fluxes, J. Geophys. Res. 71, 1-28 (1966). http://dx.doi.org/10.1029/JZ071i001p00001

Kim EH, Johnson JR, Full-wave modeling of EMIC waves near the He+ gyrofrequency, Geophys. Res. Lett. submitted (2015).

Kim EH, Lee DH, Resonant absorption of ULF waves near the ion cyclotron frequency: A simulation study, Geophys. Res. Lett. 30, 2240 (2003). http://dx.doi.org/10.1029/2003GL017918

Kim EH, Johnson JR, Lee DH, Resonant absorption of ULF waves at Mercury's magnetosphere, J. Geophys. Res. 113, A11207 (2008). http://dx.doi.org/10.1029/2008JA013310

Kim EH, Johnson JR, Lee KD, ULF wave absorption at Mercury, Geophys. Res. Lett. 38, L16111 (2011a). http://dx.doi.org/10.1029/2011GL048621

Kim EH, Johnson JR, Lee DH, Pyo YS, Field-line resonance structure in Mercury's multi-ion magnetosphere, Earth Planets Space 65, 447-451 (2013). http://dx.doi.org/10.5047/eps.2012.08.004

Kim EH, Johnson JR, Valeo E, Phillips CK, Global modeling of ULF waves at Mercury, Geophys. Res. Lett. 42, 5147–5154 (2015a). http://dx.doi.org/10.1002/2015GL064531

Kim EH, Boardsen S, Johnson JR, Slavin JA, ULF waves at Mercury, in Low-frequency Waves in Space Plasmas, eds. Keiling A, Lee DH, Nakariakov V (American Geophysical Union, Washington, D.C., in press 2015b).

Kim EH, Johnson JR, Kim H, Lee DH, Inferring Magnetospheric Heavy Ion Density using EMIC waves, J. Geophysics. Res. 120, 6464-6473 (2015c). http://dx.doi.org/10.1002/2015JA021092

Kim H, Lessard MR, Engebretson MJ, Luhr H, Ducting characteristics of Pc 1 waves at high latitudes on the ground and in space, J. Geophys. Res. 115, A09310 (2010). http://dx.doi.org/10.1029/2010JA015323

Kim H, Lessard MR, Engebretson MJ, Young MA, Statistical study of Pc1–2 wave propagation characteristics in the high-latitude ionospheric waveguide, J. Geophys. Res. 116, A07227 (2011b). http://dx.doi.org/10.1029/2010JA016355

Klimushkin DY, Mager PN, Glassmeier KH, Axisymmetric Alfven resonances in a multi-component plasma at finite ion gyrofrequency, Ann. Geophys. 24, 1077-1084 (2006). http://dx.doi.org/10.5194/angeo-24-1077-2006

Klimushkin DY, Mager PN, Marilovtseva OS, Parallel structure of Pc1 ULF oscillations in multi-ion magnetospheric plasma at finite ion gyrofrequency, J. Atmos. Sol.-Terr. Phys. 72, 1327-1332 (2010). http://dx.doi.org/10.1016/j.jastp.2010.09.019

Lee DH, Lysak RL, Magnetospheric ULF wave coupling in the dipole model - The impulsive excitation, J. Geophys. Res. 94, 17097-17103 (1989). http://dx.doi.org/10.1029/JA094iA12p17097

Lee DH, Johnson JR, Kim K, Kim KS, Effects of heavy ions on ULF wave resonances near the equatorial region, J. Geophys. Res. 113, A11212 (2008). http://dx.doi.org/10.1029/2008JA 013088

Lee DH, Lee DY, Shin DK, Kim JH, Cho JH, A Statistical Test of the Relationship Between Chorus Wave Activation and Anisotropy of Electron Phase Space Density, J. Astron. Space Sci. 31, 295-301 (2014). http://dx.doi.org/10.5140/JASS.2014.31.4.295

Othmer C, Glassmeier KH, Cramm R, Concerning field line resonances in Mercury's magnetosphere, J. Geophys. Res. 104, 10369-10378 (1999). http://dx.doi.org/10.1029/1999JA900009

Raines JM, Gershman DJ, Slavin JA, Zurbuchen TH, Korth H, et al., Structure and dynamics of Mercury'smagnetospheric cusp: MESSENGER measurements of protons and planetary ions, J. Geophys. Res. 119, 6587-6602 (2014). http://dx.doi.org/10.1002/2014JA020120

Rauch JL, Roux A, Ray tracing of ULF waves in a multicomponent magnetospheric plasma - Consequences for the generation mechanism of ion cyclotron waves, J. Geophys. Res. 87, 8191-8198 (1982). http://dx.doi.org/10.1029/JA087iA10p08191

Russell CT, Khurana KK, Arridge CS, Dougherty MK, The magnetospheres of Jupiter and Saturn and their lessons for the Earth, Adv. Space Res. 41, 1310-1318 (2008). http://dx.doi.org/10.1016/j.asr.2007.07.037

Song SH, Lee DH, Pyo YS, Wave Model Development in Multi-Ion Plasmas, J. Astron. Space Sci. 16, 41-52 (1999).

Taylor WWL, Lyons LR, Simultaneous equatorial observations of 1- to 30-Hz waves and pitch angle distributions of ring current ions, J. Geophys. Res. 81, 6177-6183 (1976). http://dx.doi.org/10.1029/JA081i034p06177

Vincena ST, Farmer WA, Maggs JE, Morales GJ, Laboratory realization of an ion-ion hybrid Alfvén wave resonator, Geophys. Res. Lett. 38, L11101 (2011). http://dx.doi.org/10.1029/2011GL047399

Vincena ST, Farmer WA, Maggs JE, Morales GJ, Investigation of an ion-ion hybrid Alfvén wave resonator, Phys. Plasmas 20, 012111 (2013). http://dx.doi.org/10.1063/1.4775777

Williams DJ, Lyons LR, Further aspects of the proton ring current interaction with the plasmapause: Main and recovery phases, J. Geophys. Res. 79, 4791-4798 (1974a). http://dx.doi.org/10.1029/JA079i031p04791

Williams DJ, Lyons LR, The proton ring current and its interaction with the plasmapause: Storm recovery phase, J. Geophy. Res. 79, 4195-4207 (1974b). http://dx.doi.org/10.1029/JA079i028p04195

Zurbuchen TH, Raines JM, Slavin JA, Gershman DJ, Gilbert JA, et al., MESSENGER observations of the spatial distribution

of planetary ions near Mercury, Science 333, 1862-1865 (2011). http://dx.doi.org/10.1126/science.1211302